J2.5 A Comparison of Zonal Moisture Variability Derived from GPS/MET Occultation Observations and ECMWF Analyses from June 21-July 4, 1995

E. R. Kursinski(1,2), G. A. Hajj(2), D. Hankins(1), C. O. Ao(2), B. A. Iijima(2), L. J. Romans(2), M. de la Torre Juarez(2), D. Wu(2)

[1]Department of Atmospheric Sciences, University of Arizona
[2]Jet Propulsion Laboratory, California Institute of Technology

Extended Abstract for AMS 2003
Long Beach, CA, February 2003
Submitted October 2002

Abstract

Moisture concentrations in the troposphere are determined to first order by temperature via saturation and condensation. However, most of the tropospheric volume is significantly below saturation on average implying the controlling influence of temperature must occur in general during excursions from mean conditions. Therefore characterization of variability is important in understanding moisture control mechanisms. Here we characterize zonal moisture variability derived from occultation observations of Global Positioning System (GPS) satellites made by GPS/MET in June-July 1995 [*Ware et al.,* 1996] combined with European Centre for Medium-Range Weather Forecasts (ECMWF) temperature analyses and compare the results with the ECMWF global humidity analyses. The zonal variability estimates are similar but substantial differences exist particularly between the individual moisture profiles. Our analysis of the errors in the two moisture data sets suggests that the accuracy of the ECMWF moisture analyses in the Northern Hemisphere is similar to that represented in the analysis error covariances but the ECMWF moisture analyses in the Southern Hemisphere are significantly less accurate. We also find that significant correlations exist between the errors and true moisture variations through most of the troposphere. The sign of the correlation is consistent with the ECMWF analyses smoothing out a significant fraction of the vertical variations in the moisture field. Variability at low latitudes is larger in the GPS results suggesting variations exist at vertical scales resolved by the occultations but not by TOVS and the ECMWF analyses. In the winter hemisphere baroclinic zone, ECMWF variability is larger and may be overestimated in the ECMWF analyses.

Using our error and correlation estimates we derive an optimal weighting for combining the occultation and ECMWF moisture information. The inclusion of the GPS data should reduce the analysis errors by more than 50% over most of the lower half of the troposphere. The impact of the GPS data is larger in the winter hemisphere than expected because the ECMWF errors are larger there. The meridional and height dependence of the zonal variability of moisture exhibits a distinct bimodal distribution with a minimum near ITCZ and a relative maximum to either side, similar to that discussed by *Peixoto and Oort* [1992] but with a greater magnitude. The two relative maxima are associated with longitudinal variability across the subtropics as well as the monsoons in the Northern Hemisphere. Above ~3 km altitude, moisture variations are $\geq$ 50% of the mean in Northern (summer) Hemisphere and $\geq$ 70% of the mean in the Southern (winter) Hemisphere.

1. INTRODUCTION

Tropospheric moisture concentrations are controlled to first order by temperature via the Clausius-Clapeyron relation. Variations in tropospheric moisture are of the order of the mean moisture and therefore vary by several orders of magnitude over the vertical extent of the troposphere. Since most of the tropospheric volume is not continuously filled by clouds, the control exerted by temperature via saturation must in general occur during excursions from mean conditions. Therefore characterization of moisture variability represents an important aspect of understanding moisture control mechanisms. Present understanding and model representations of these mechanisms typically limits weather predictions of atmospheric moisture to 12 hours or less, a limitation which raises fundamental doubts about the accuracy of free-running climate models. Improvements in control mechanisms will improve precipitation predictions as well as our understanding of the present climate system and the evolution of the system under anthropogenic changes in forcing. Further, knowledge of variability provides direct constraints in assessing the climate model accuracy.

The small spatial and temporal scales over which water varies make accurate observations of atmospheric moisture from space difficult such that even the mean distribution of moisture is not well characterized globally. Accurate determination of variance, a second moment, presents an even greater challenge. Here we discuss the zonal variability of water vapor derived from occultation observations of the Global Positioning System (GPS) satellites and the global ECMWF humidity analyses.

In a radio occultation, the limb-viewing geometry yields profiles of the index of refraction, n, with a vertical resolution of 0.2 to 1 kilometer in the troposphere at long 20 cm wavelengths capable of penetrating aerosols, clouds and precipitation [*Kursinski et al.* 1997]. The principal observable is the additional propagation delay due to the reduction of the speed of light in the atmosphere relative to vacuum. The time rate of change of the additional delay is directly related to the bending angle from which n is derived as a function of radius. *Smith and Weintraub* [1953] showed that atmospheric refractivity, defined as $N = (n\text{-}1) \times 10^6$, at microwave wavelengths can be written as

$$N = b_1 \frac{P}{T} + b_2 \frac{P_w}{T^2} \tag{1}$$

where P and P_w are total pressure and partial pressure of water vapor respectively in mbar, T is temperature in K, b_1 is 77.6 N-units K mbar^{-1} and b_2 is 3.73x10^5 N-units K^2 mbar^{-1}. The first and second terms on the RHS are due primarily to the polarizability of the molecules and the permanent dipole moment of the water vapor molecule respectively. The partial pressure of water vapor derived from refractivity is

$$P_w = \frac{T(NT - b_1 P)}{b_2} \tag{2}$$

Similarly, specific humidity, the mass mixing ratio of water vapor, q, is

$$q = \left[\frac{m_w}{m_d} \left(\frac{b_2 P}{T(NT - b_1 P)} - 1 \right) + 1 \right]^{-1} \tag{3}$$

where m_w and m_d are the mean molecular masses of water vapor and dry air respectively.

To derive P_w and q from (2) and (3), refractivity, temperature and pressure must be known. Refractivity is derived directly from the occultation observations and pressure and temperature are related hydrostatically leaving one equation and two unknowns. The wet and dry contributions to refractivity cannot be separated from the GPS observations alone because refractivity at microwave wavelengths is non-dispersive. The additional constraint used here to derive water vapor is temperature from the nearest 6 hour global ECMWF analysis interpolated to each occultation location. A more in depth discussion of the processing of the occultation data to derive moisture is described in *Kursinski and Hajj* [2001]. We refer to water vapor derived in this fashion as GPS-ECMWF Water vapor (GE) and the interpolated ECMWF analyses as IE. It is important to note that humidity derived from GPS refractivity and an additional constraint on temperature is absolute rather than relative humidity.

GPS occultation observations commenced with the launch of GPS/MET in April 1995. GPS/MET data acquired from June 21 to July 4, 1995 (referred to as JJ95) has the best qualities acquired by GPS/MET for studying moisture. In the present study we utilize the GPS and ECMWF data sets from JJ95 to characterize globally the zonal variance of specific humidity as well as the variance of the errors in the GE and ECMWF humidity data sets. The differing resolutions of these two datasets allow insight into their respective accuracies as well as the true variability of moisture at the resolution scales or larger. Variations at smaller scales are essentially invisible to the present study.

The paper is structured as follows. Section 2 is a discussion of the zonal variability of moisture in the GE and IE data sets. In section 3 we examine the errors in the GE and IE data sets including cross-correlations between the errors and the errors and true moisture variations which we find are significant. In Section 4, we utilize our knowledge of errors we derive and derive a best estimate of zonal moisture variability during the JJ95 period as well as an indication of the impact GPS should have on global moisture analyses. In Section 5 we interpret the results utilizing the improved understanding of errors developed in Section 3. We summarize and conclude in section 6.

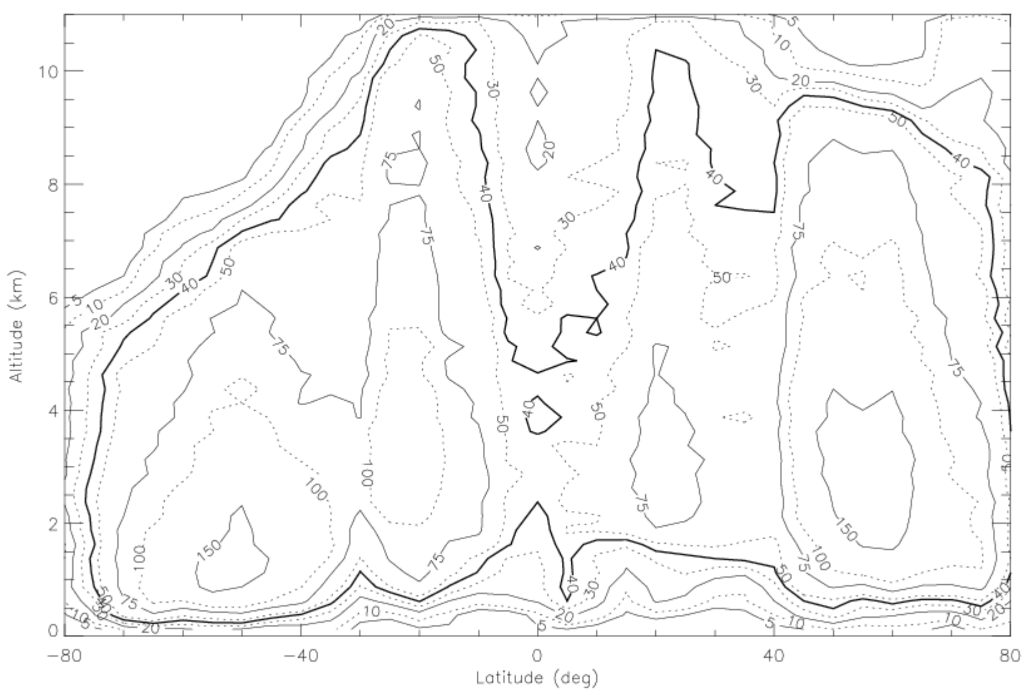

Figure 1: Contours of number of occultation points in each latitude-height bin

2. RESULTS

Since the GPS/Met data set used here is too small to derive a statistically robust characterization of global 3-D moisture structure, we have reduced the moisture data into a 2-D, latitude versus height grid that retains the vertical and meridional gradients. Grid boxes are 250 meters high spaced every 250 meters in height. Each box is 10 degrees of latitude wide spaced every 5 degrees of latitude. The number of occultation profile points in each latitude height bin shown in Figure 1 ranges from less than 20 to more than 150. The mean moisture in each grid box is an estimate of the zonal mean at that height and latitude which has been discussed by *Kursinski and Hajj* [2001]. In this two dimensional representation, the variance of specific humidity estimates in each grid box is the variance of the zonal moisture fluctuations about the zonal mean.

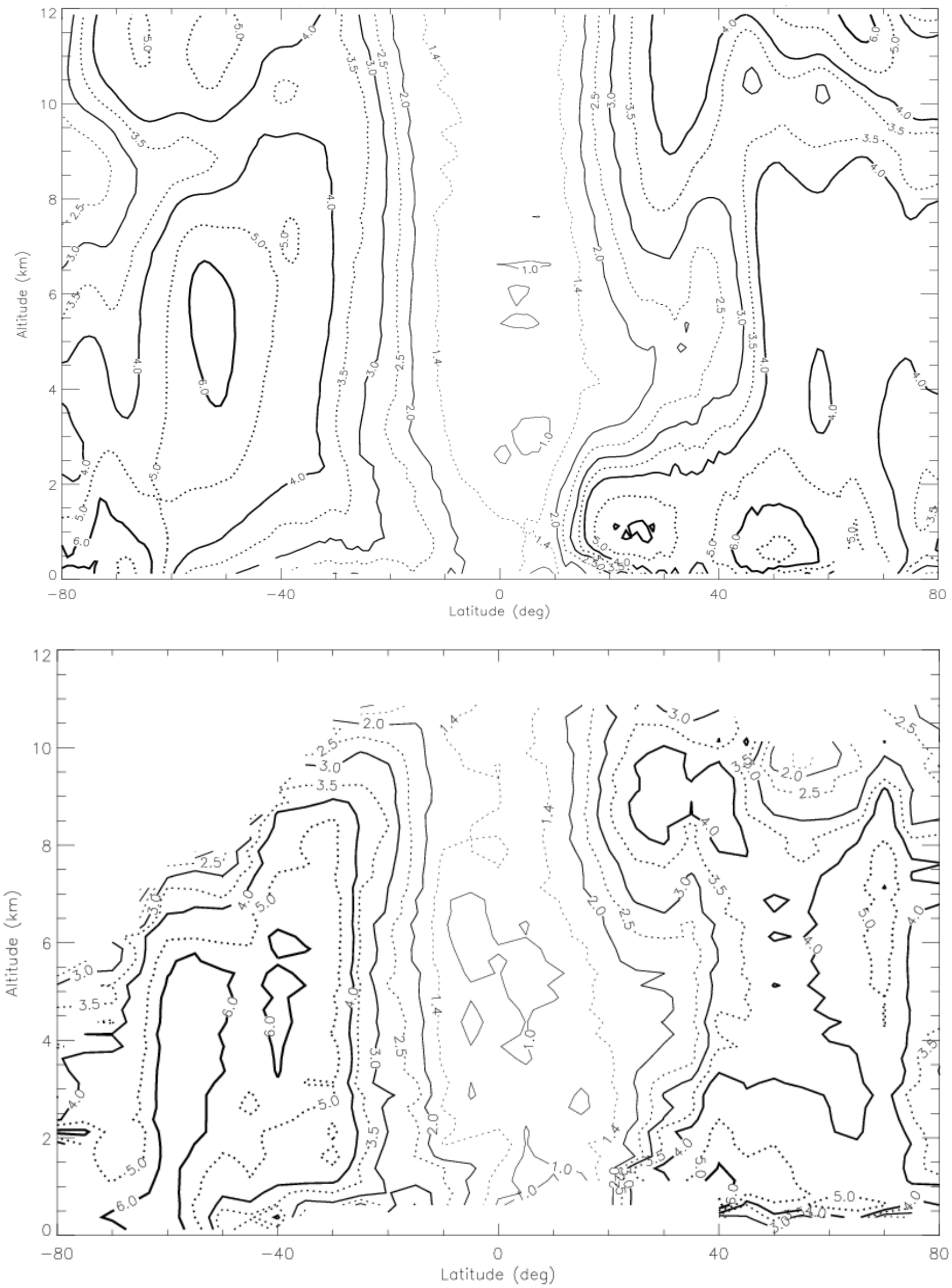

Figure 2: Zonal variability of ECMWF temperatures in (K). a. The complete ECMWF analyses for JJ95. b. The subset of the ECMWF analyses interpolated to the GPSMET occultation locations.

The structure of standard deviation of the ECMWF analysis temperatures relative to the zonal mean (σ_T) is shown in Figure 2. Low latitude zones exhibit the least variability of 1 to 1.4 K. Maximum variability as large as 6 K is found in the Southern Hemisphere in the high baroclinicity winter region between 30^{o}S and 60^{o}S. Variability in the Northern Hemisphere reaches a maximum of 4 to 5 K north of 50N. Variability in the zone from 20^{o}N to 40^{o}N exhibits a distinct vertical dependence with near-surface and upper troposphere maxima and a minimum near 5 km altitude associated with the summer monsoons in this zone. With a few exceptions, the complete ECMWF (CE) and ECMWF interpolated to the GPS occultation locations (IE) results are in general agreement although noisier than the mean comparison [*Kursinski and Hajj*, 2001]. In the structure between 20^{o}N and 40^{o}N, the similarity of the CE and IE σ_T structure above 2 km indicates the GPS sampling has captured the behavior above 2 km. Within 1.5 km of the surface, the smaller variability exhibited in the IE data probably indicates the reduced number of occultations reaching that altitude regime (Figure 1) do not capture the entire range of behavior there.

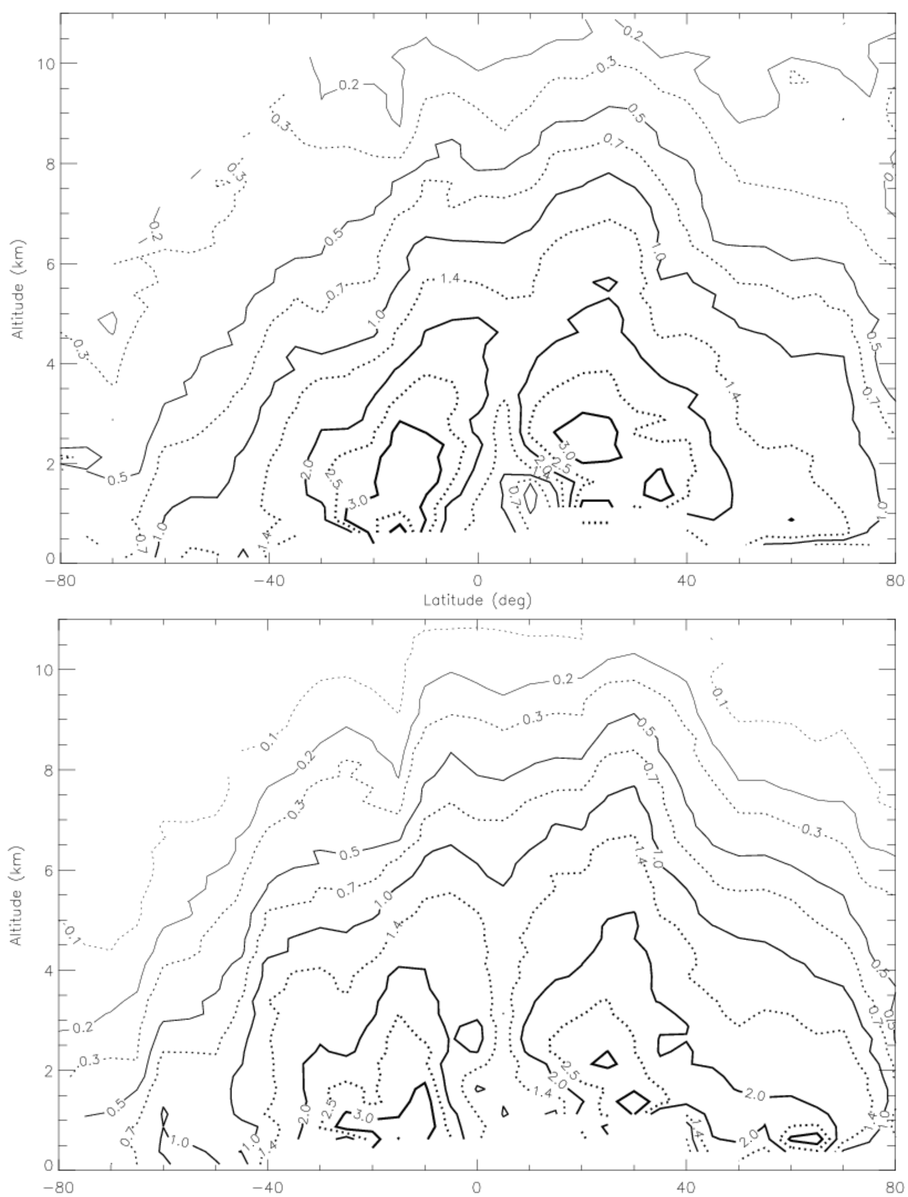

Figure 3. Standard deviation of specific humidity variations about the zonal mean (in g/kg). a. Specific humidity derived from GPS/MET refractivities and ECMWF temperatures. b. ECMWF specific humidity analyses.

Figures 3a and 3b show the standard deviation of specific humidity variations about the zonal mean derived from the GPS refractivity using the ECMWF temperatures (GE) and Interpolated ECMWF (IE) data sets respectively. The similarity of the two estimates of zonal variability structure implies both data sets have captured the same first order zonal behavior. The difference in the variances and the fractional variance differences (Figures 4a and 4b) reveal large regional differences between the two variance estimates. Given the differences in the resolution particularly in the vertical dimension between the GPS occultation data and the TOVS data assimilated in the analyses, the differences also indicate a subset of the spatial scales over which water varies.

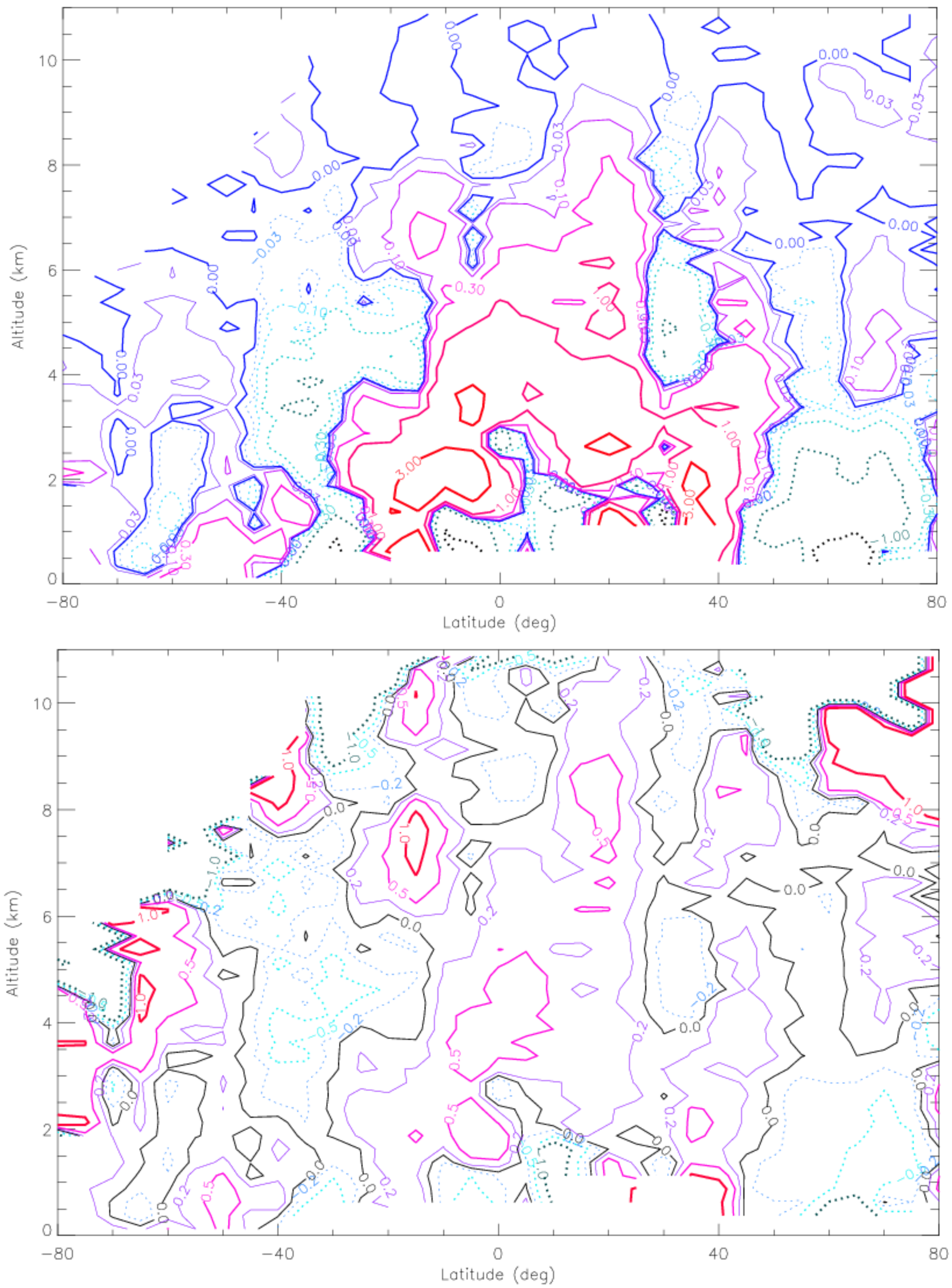

Figure 4: Difference between zonal variance of specific humidity estimates, GPS minus ECMWF.
a. $\sigma_{qG}^2 - \sigma_{qE}^2$ in $(g/kg)^2$. b. fractional difference: $\sigma_{qG}^2 - \sigma_{qE}^2$ normalized by $(\sigma_{qG}^2 + \sigma_{qE}^2)/2$

3. ERRORS IN THE SPECIFIC HUMIDITY ESTIMATES

In this section we attempt to separate the errors in the GE and IE moisture estimates from the true variability. We are able to estimate the GE errors and the IE errors but we have to add additional constraints beyond the data alone because we find that the correlations between the errors and true variability are significant. A major finding is the ECMWF moisture estimates are 2 to 3 times less accurate in the Southern hemisphere.

There are several steps involved in isolating the errors. We first write the observed specific humidity in terms of the true specific humidity plus errors and further divide each of these into their mean and variable contributions. We then write and calculate the three linear combinations of the obervations that would separate the true variability from that of the GE and IE moisture errors if the correlations were small. However, upon examination of the results, we find immediately that significant correlations must exist between the data sets, leaving us with 3 equations and 6 unknowns. Therefore direct separation of the error terms and true moisture variability from the data alone is not possible. To make further progress, we develop two additional constraints. First we estimate the error in the ECMWF analysis temperatures in the upper troposphere in order to estimate the error in the GPS moisture estimates via the approach of *Kursinski et al.* [1995] and *Kursinski and Hajj* [2001]. The second constraint is the cross correlation of the GPS and ECMWF moisture errors which we can estimate from the temperature errors common to the GE and IE moisture data sets. Given these two constraints plus those of the data itself, we estimate the error in the ECMWF humidity analyses and find the analyses are significantly less accurate in the Southern Hemisphere. We are also able to estimate the difference between the correlation of the GPS moisture errors with the true moisture variations and the correlation of the ECMWF errors with the true moisture variations. The sign of this difference suggests the moisture in the ECMWF analyses is significantly smoothing out vertical moisture structure.

3.1 Separation of Errors

Each specific humidity estimate can be decomposed into truth plus an error such that the q from IE ($\equiv q_E$) and that derived from GPS refractivity plus the ECMWF temperatures ($\equiv q_G$) can be written as

$$q_E = \overline{q} + q' + \overline{\varepsilon_E} + \varepsilon_E' \tag{4a}$$

$$q_G = \overline{q} + q' + \overline{\varepsilon_G} + \varepsilon_G' \tag{4b}$$

where ε_E and ε_G are the errors in the IE and GE estimates of q and overbars and primes refer to the zonal mean and variable parts of each term respectively. The variance of the IE and GE q estimates and their differences can therefore be written as

$$\sigma_{qE}^2 = \overline{q'^2} + 2\,\overline{q'\varepsilon'_E} + \overline{\varepsilon'^2_E} \tag{5a}$$

$$\sigma_{qG}^2 = \overline{q'^2} + 2\,\overline{q'\varepsilon'_G} + \overline{\varepsilon'^2_G} \tag{5b}$$

Another observable that we can readily estimate is the difference between the q estimates ($\equiv$ Δq) which is defined as

$$\Delta q = q_G - q_E = \overline{\varepsilon_G} + \varepsilon'_G - \overline{\varepsilon_E} - \varepsilon'_E$$

The variance of Δq is

$$\sigma_{\Delta q}^2 = \overline{\varepsilon'^2_G} - 2\,\overline{\varepsilon'_G\varepsilon'_E} + \overline{\varepsilon'^2_E} \tag{6}$$

Figure 5 shows the behavior of $\sigma_{\Delta q}$ normalized by the zonally averaged q. Perhaps the most striking feature of Figure 5 is dramatic difference between the magnitude of the discrepancies in the Northern and Southern Hemispheres with the Southern Hemisphere discrepancies being 2 or more times larger than those in the Northern Hemisphere. This hemispheric discrepancy is in fact what motivated the present work.

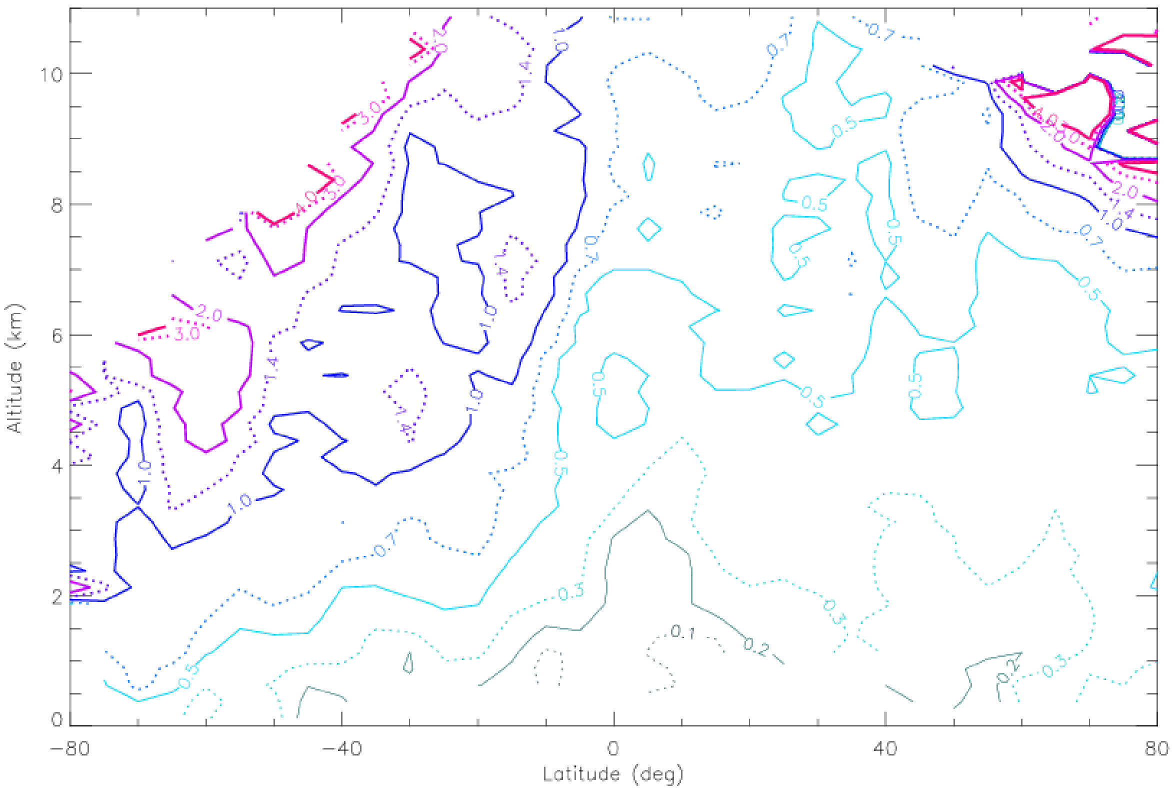

Figure 5: The normalized standard deviation of the zonal variations in the difference between the individual GPS and ECMWF moisture profiles, $(=\sigma_{\Delta q}/\overline{q})$.

(5a), (5b) and (6) provide three constraints sufficient to isolate the true variability, the error in the q_G estimates and the error in the q_E estimates ***if*** the cross-correlation terms are small. Three combinations that would do so are

$$\frac{1}{2}\left(\sigma_{qE}^2+\sigma_{qG}^2-\sigma_{\Delta q}^2\right) = \overline{q'^2}+\overline{q'\varepsilon'_E}+\overline{q'\varepsilon'_G}+\overline{\varepsilon'_E\varepsilon'_G} \tag{7a}$$

$$\frac{1}{2}\left(\sigma_{qE}^2-\sigma_{qG}^2+\sigma_{\Delta q}^2\right) = \overline{\varepsilon'^2_E}+\overline{q'\varepsilon'_E}-\overline{q'\varepsilon'_G}-\overline{\varepsilon'_E\varepsilon'_G} \equiv L_E \tag{7b}$$

$$\frac{1}{2}\left(-\sigma_{qE}^2+\sigma_{qG}^2+\sigma_{\Delta q}^2\right) = \overline{\varepsilon'^2_G}-\overline{q'\varepsilon'_E}+\overline{q'\varepsilon'_G}-\overline{\varepsilon'_E\varepsilon'_G} \equiv L_G \tag{7c}$$

The behavior of (7a) (not shown) is similar to that in Figures 3a and 3b as expected since (7a) is a third estimate of the true variance with a different combination of noise contributions from those in (5a) and (5b).

Figure 6 shows the behavior of L_E defined in (7b). Perhaps the most significant feature of Figure 6 is that it contains significant regions where L_E is negative. In these regions, the net contribution of the correlation terms in (7b) must be negative and greater in magnitude than the variance of the ECMWF moisture analysis errors. Therefore the correlation terms are large and cannot be ignored. As a result, we find ourselves with three equations (7a), (7b), and (7c) and six unknowns and cannot use the data alone to separate the true specific humidity variance and the variance of the ECMWF and GPS noise contributions. To make further progress we must add some additional constraints. We are in fact able to add two further constraints and separate 5 of the 6 terms in (7a), (7b), and (7c).

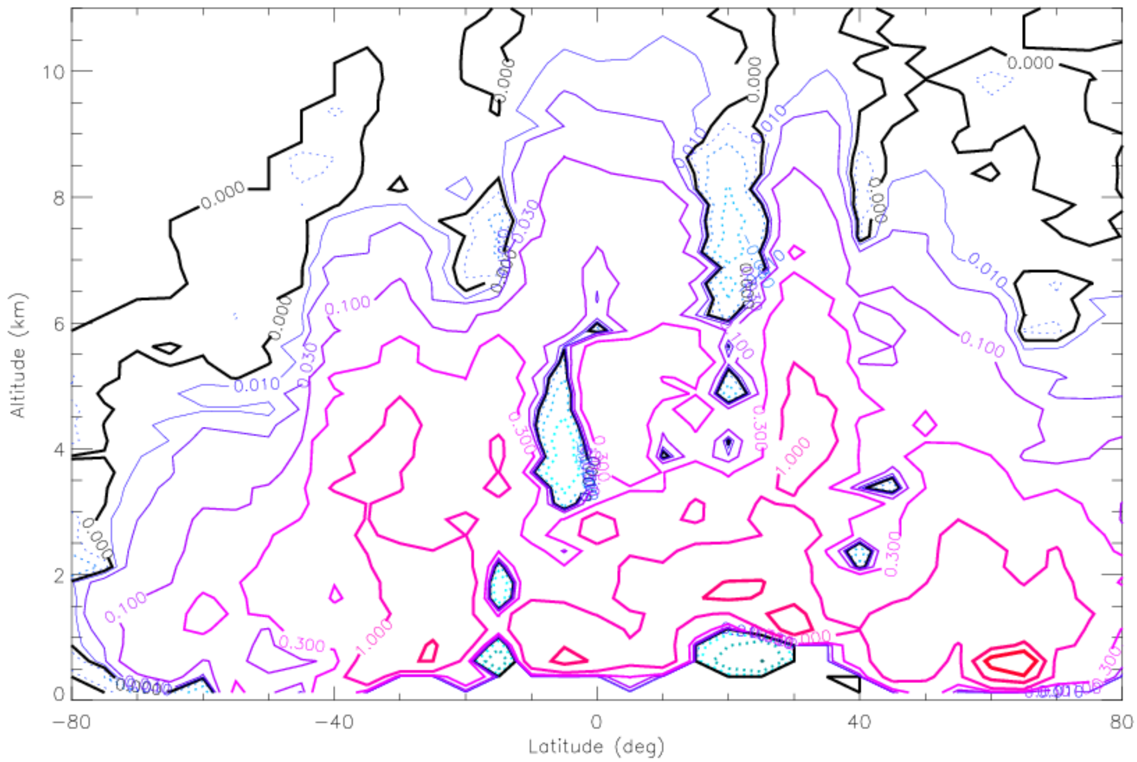

Figure 6: Zonal behavior of L_E defined in (7b) in $(g/kg)^2$.

3.2 High altitude estimate of σ_{qG} and equivalent temperature error

In trying to estimate the terms in (7a), (7b), and (7c), one additional constraint comes from applying the analysis of *Kursinski et al.* [1995] to estimate the accuracy of the GPS moisture estimates. *Kursinski et al.* [1995] estimated the accuracy of water vapor derived from GPS-derived refractivity when temperatures were provided from an independent source such as a weather analysis. The error in water vapor derived in this manner has two primary sources, temperature errors which dominate at higher altitudes and refractivity errors which can become dominant at low altitudes. [*Kursinski and Hajj*, 2001] modified the results of *Kursinski et al.* [1995] to show that the fractional error in specific humidity is related to fractional errors in refractivity, temperature and pressure as defined in (8).

$$\frac{dq}{q} \cong (B+1)\frac{dN}{N} + (B+2)\frac{dT}{T} - (B+1)\frac{dP}{P} \tag{8}$$

$$\text{where } B = \frac{b_1\,T\,P}{b_2\,P_w} \cong \frac{b_1\,T\,m_w}{b_2\,q\,m_d}.$$

m_d and m_w are the mean molecular weights of dry air and water vapor respectively. The temperature error ($\equiv \varepsilon_T$) at high altitudes where B>>1 causes an error in q ($\equiv \varepsilon_q$) equal to

$$\varepsilon_q \cong \frac{b_1\,m_w}{b_2\,m_d}\,\varepsilon_T \tag{9}$$

indicating that the variance of the error in the GPS moisture results approaches an asymptotic value at high altitudes. In contrast, since moisture variability is of the order of the mean humidity, the absolute (as opposed to fractional) variability of tropospheric specific humidity must decrease dramatically with increasing altitude. Therfore, as altitude increases, the variance of errors in the GPS-derived specific humidity becomes much larger than the true moisture variance. Indeed σ_{qG} is observed to have an asymptotic limit of ~0.2 g/kg at high altitudes in Figure 3a as expected according to *Kursinski and Hajj* [2001]. Therefore, since radiances are more directly related to relative humidity [*Soden and Bretherton*, 1996], analyses assimilating TOVS moisture radiances should provide a better estimate of σ_q than σ_{qG} at high altitudes at least up to altitudes where the TOVS radiances are sensitive to moisture. We can therefore utilize the high altitude differences between the GE and IE moisture variances as a measure of the variance of GE specific humidity errors and then use the approach of *Kursinski and Hajj* [2001] to estimate the high altitude asymptotic error in q and the equivalent temperature inconsistency.

The temperature inconsistency equivalent to the specific humidity difference is derived as follows. Consider the situation where q_E is known as are the GPS refractivity, N_G, and the GPS pressure, P_G. We can define an equivalent temperature, T_{EG}, which is the temperature that is consistent with the observed values of q_E, N_G and P_G and the refractivity equation. In addition we have the estimate of q_G derived from N_G and P_G and the ECMWF temperatures, T_E. Using (8), we can relate the difference between the two moisture estimates to the difference between the two temperatures as

$$\frac{q_E - q_G}{q} = \frac{\varepsilon_{q_E} - \varepsilon_{q_G}}{q} = (B+2)\frac{\varepsilon_{T_E} - \varepsilon_{T_{EG}}}{T}$$

Since the GPS refractivities have small fractional errors at high altitudes, the error in q_G at high altitudes is dominated by the ECMWF temperature error. On the other hand, at high altitudes, the errors in q_E should be smaller than the errors in q_G because the q_E errors are proportional to q which decreases at high altitudes. Therefore, at sufficiently high altitudes, $\varepsilon_{T_E} - \varepsilon_{T_{EG}} \approx \varepsilon_{T_E}$ and

$$\sigma_{TE} \cong \sigma_{\Delta q}\frac{T}{q(B+2)} \cong \sigma_{\Delta q}\frac{b_2 m_d}{b_1 m_w} \tag{10}$$

In the derivation of water vapor from refractivity discussed here, pressure is the occultation-derived hydrostatic pressure above the 230K temperature altitude plus the hydrostatic contribution of the analysis temperatures at lower altitudes. The impact of analysis temperature errors on derived pressure are therefore small at altitudes within roughly a half scale height of the 230K height. Therefore the high altitude inconsistency in q is essentially equivalent to an inconsistency between the GPS and ECMWF temperature estimates.

Figure 7 shows the standard deviation of the equivalent temperature inconsistency derived along the 237K mean temperature contour. Overall, the result is similar to the temperature uncertainty of 1.5 K generally assumed for global analyses and assumed in the GPS water vapor accuracy prediction of *Kursinski et al.* [1995]. At low latitudes where temperature variability is small, agreement is better, being approximately 1 K. Larger discrepancies of between 1.5 and 2.5 K are found at higher latitudes in the Southern Hemisphere. *Kursinski and Hajj* [2001] found regions where the mean GE relative humidity is negative which implies mean square temperature errors of the ECMWF analyses are ~2.8K. The errors estimated here are somewhat smaller but generally in agreement with that estimate lending support to the temperature error estimates made here.

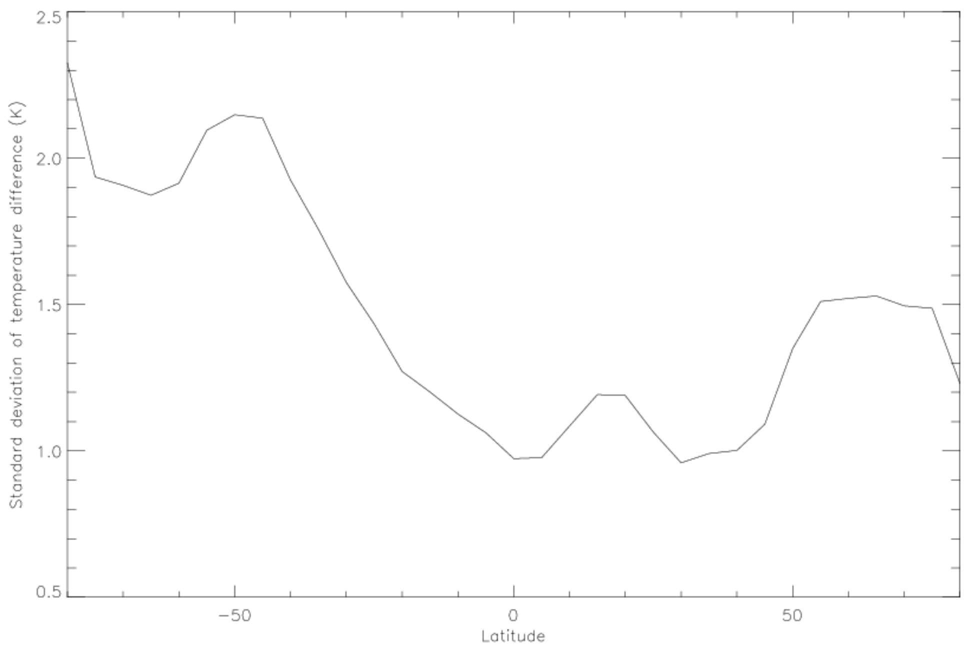

Figure 7: Estimated standard deviation of ECMWF temperature errors as a function of latitude

There is a problem in our temperature error estimation approach near 35°N where the GE and IE moisture variances are approximately equal. The temperature inconsistency at this zone is probably similar to that of the surrounding latitudes and we have smoothed latitudinally to reduce this effect.

3.3 Estimation of $\overline{\varepsilon_G^{'2}}$

Given our estimates of the ECMWF temperature errors, we can proceed to estimate $\overline{\varepsilon'^2_G}$, the variance of the errors in q_G. We follow the approach of *Kursinski et al*. [1995] who showed the dominant error contribution in upper regions is due to the analysis temperature errors whereas in lower moist regions, refractivity errors can become dominant. From (8), the GE specific humidity error variance is related to the temperature and refractivity error variances approximately as

$$\frac{\overline{\varepsilon'^2_{qG}}}{q^2} \cong (B+1)^2 \frac{\overline{\varepsilon'^2_{NG}}}{N^2} + (B+2)^2 \frac{\overline{\varepsilon'^2_{TE}}}{T^2}$$

We have assumed the errors in the GPS refractivity and ECMWF analysis temperatures are independent and, as in *Kursinski et al.* [1995], we have ignored the contribution of the pressure error because it is generally small. In applying the temperature errors shown in Figure 7, we assume the standard deviation of the temperature error does not vary significantly with height.

Kursinski et al. [1995] and *Healy* [2001] found that the fractional refractivity error increased at lower altitudes because of the associated increase in horizontal refractivity variations which cannot be represented in the abel transform. The increase was approximately in proportion to the increase in specific humidity at lower altitudes. To take this effect into account, we approximate the fractional refractivity error as

$$\frac{\overline{\varepsilon_{NG}^{'2}}}{N^2} = \left[\left(3x10^{-3}\,\overline{q}\right)^2 + \left(2x10^{-3}\right)^2\right]^{1/2} \qquad (12)$$

where q is in g/kg. (12) yields refractivity errors somewhat larger than those estimated by *Kursinski et al.* [1995] in the lower troposphere in order to account for possible receiver tracking errors. We truncate (12) at a maximum refractivity error of 2% which is twice the maximum refractivity error in the lower troposphere estimated by *Kursinski et al*. [1995]. We note that our estimate of the GPS refractivity errors may be conservative in the Northern Hemisphere summer where *Poli et al.* [2002] found indications that the results of *Kursinski et al*. were pessimistic.

The resulting latitude versus height dependence of $\overline{\varepsilon'^2_G}$ normalized by $\bar{q}$ is shown in Figure 8. Fractional accuracy is lower in the Southern Hemisphere reflecting the lower mean specific humidities and larger temperature errors there. At low latitudes, the fractional errors reach a minimum because of the high mean humidities and relatively small temperature errors.

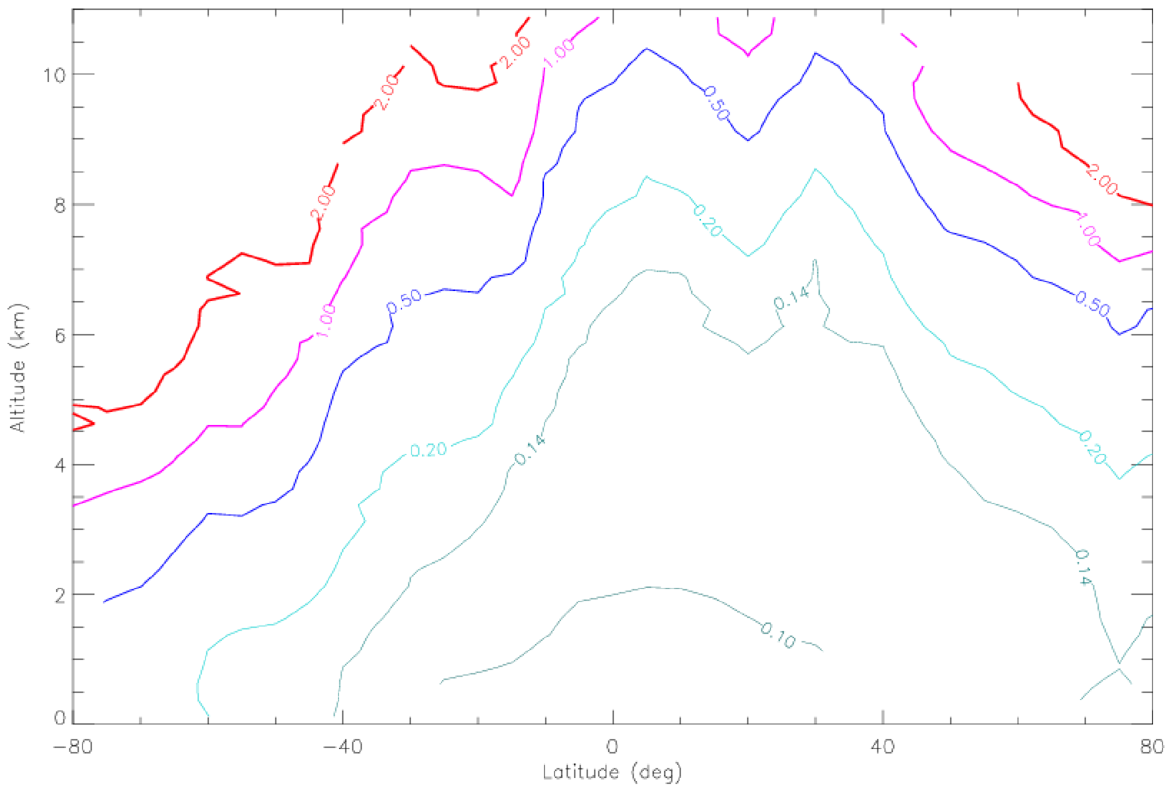

Figure 8: Estimated fractional standard deviation of GPS specific humidity errors

3.4 Cross-correlation between errors: $\overline{\varepsilon'_G \varepsilon'_E}$

We have one other constraint we can apply because we know the ECMWF and GPS moisture estimates should be correlated because the ECMWF temperature estimates are common to both moisture estimates. At high altitudes, L_E is negative at most latitudes. The cause of this is probably related to the large error in the q_G estimates at high altitudes as discussed in section 3.2. This further suggests that the dominant correlation term in (7b) in the high altitude regions of negative L_E involves ε_G'. In order for the $\overline{q'\varepsilon'_G}$ term to contribute significantly to the negative values of L_E observed in the upper troposphere, the ECMWF temperature errors would have to be positively correlated with the true moisture variations. A mechanism to explain this is not obvious to us. On the other hand, it is clear that ε_G' and ε_E' will be correlated because the ECMWF temperatures are common to both data sets. We can express the expected contribution of $\overline{\varepsilon'_G \varepsilon'_E}$ due to temperature errors using the relationship between TOVS radiances and relative humidity developed by *Soden and Bretherton* [1996] (see the Appendix) which is:

$$\overline{\varepsilon'_{qG}\, \varepsilon'_{qE}} = \frac{b_1\, m_w\, q}{b_2\, m} \left(\frac{1}{\beta\, T} + \frac{0.622\, L}{R\, T^2} \right) \overline{\varepsilon_T^2} \tag{A7}$$

where β is the normalized lapse rate (dln$T$/dln$P$) used by *Soden and Bretherton*. (A7) is valid to the extent that TOVS data and not radiosondes dominate the moisture analyses which is true over most of the globe and that the TOVS data and not the underlying model largely determine the analyzed moisture structure. Note that (A7) is positive in the troposphere which is the correct sign to make (7b) negative. Note also that $\overline{\varepsilon'_G \varepsilon'_E}$ scales in proportion to q, a dependence which lies between that of $\overline{\varepsilon'^2_G}$ which is approximately constant via (9) and $\overline{\varepsilon'^2_E}$ which scales crudely as $\bar{q}^2$ because TOVS radiances are proportional to relative humidity and the fractional error in q_E increases slowly with height. The proportionality to q means that at sufficiently high altitudes, $\overline{\varepsilon'_G \varepsilon'_E}$ will become greater than $\overline{\varepsilon'^2_E}$ such that L_E will become negative consistent with Figure 7.

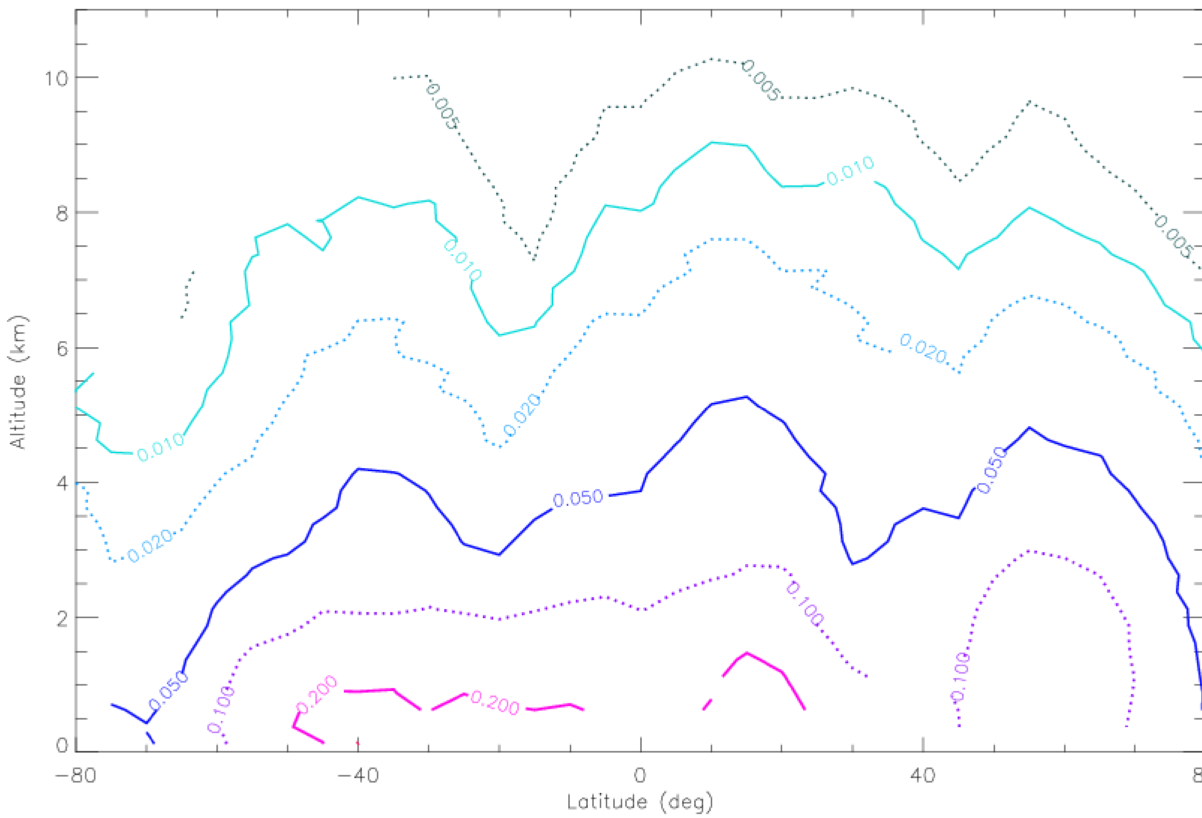

Figure 9: $\overline{\varepsilon'_G \varepsilon'_E}$ in (g/kg)^2.

To evaluate (A7) we use the meridionally varying temperature errors estimated in Figure 7 producing the $\overline{\varepsilon'_G \varepsilon'_E}$ behavior shown in Figure 9. In Figure 10 where we have added $\overline{\varepsilon'_G \varepsilon'_E}$ to L_E shown in Figure 7, we see that adding our estimate of the error cross-correlation term reduced or eliminated most of the high altitude negative regions of L_E shown Figure 7. Therefore, our simple analytic expression, (A7), seems to explain most of the high altitude correlation. Note that in deriving (A7) we assumed no correlation between T and the brightness temperature which would be incorrect if the water vapor radiances are used to constrain both constituent density and temperature in the analyses.

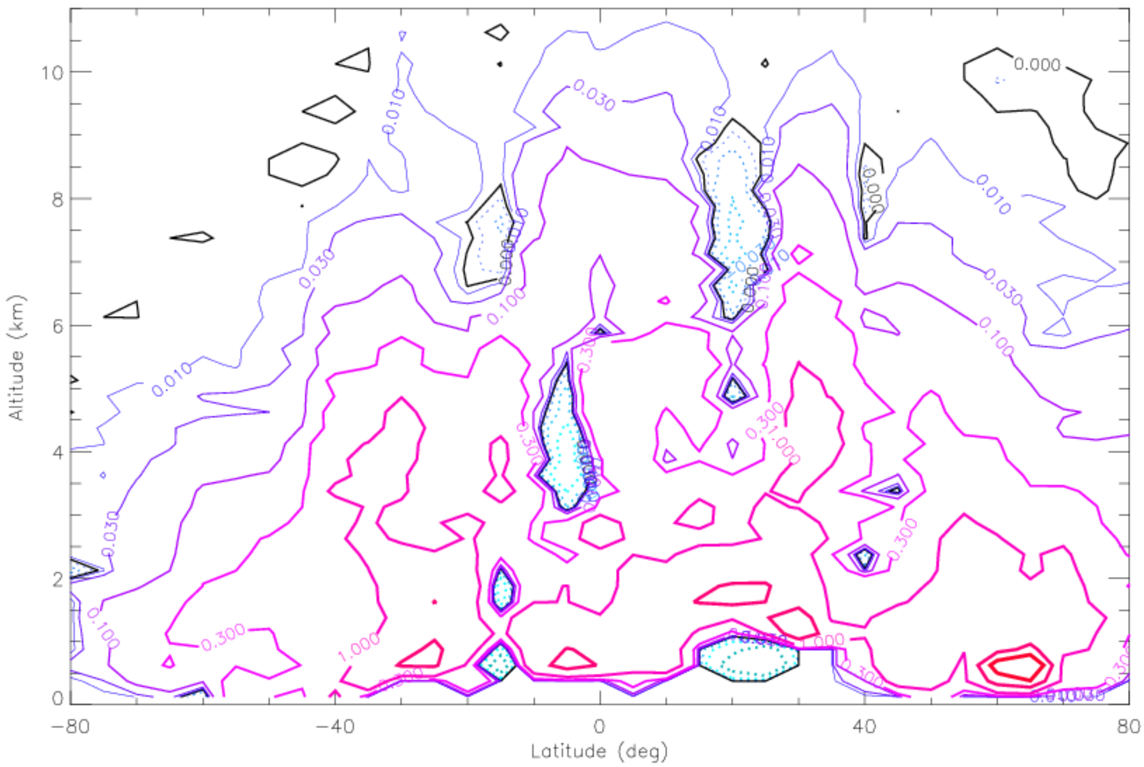

Figure 10: $L_E + \overline{\varepsilon'_G \varepsilon'_E}$ in $(g/kg)^2$.

3.5 Estimation of $\overline{\varepsilon'^2_E}$

The additional constraints of the error cross-correlation in (A7) and the estimate of $\overline{\varepsilon'^2_G}$ discussed in section 3.4 now allow us to estimate the variance of the ECMWF humidity analyses via (6). Figure 11 shows the resulting estimate of the square root of $\overline{\varepsilon'^2_E}$ normalized by $\overline{q}$. The uncertainty in the occultation-derived refractivity error in the lower troposphere in (12) and its impact on the estimate of $\overline{\varepsilon'^2_E}$ have little influence on the estimate of $\overline{\varepsilon'^2_E}$. Figure 11 reveals that the accuracy of the ECMWF analyzed moisture is distinctly worse in the Southern Hemisphere that is responsible for most of the hemispherical discrepancies evident in Figure 5.

We see that the fractional error of the ECMWF moisture is ~25% near the top of the planetary boundary layer (PBL) over much of the globe (~45°S to 60°N). North of 10°S, the ~50% accuracy contour is centered near 6 km altitude. The similarity of this to the diagonal terms of error covariances typically assigned to global moisture analyses [*e.g. Kursinski et al.*, 2000] lends credence to our result. In marked contrast, south of 10°S the fractional errors of the analyzed moisture near 6 km altitude are typically more like 100%. 50% errors in moisture are found at 1 to 2 km altitude. These results indicate that moisture errors over much of the Southern Hemisphere are factors of 2 to 3 larger than the assumed analysis errors confirming and quantifying the long-held assertion that analyzed moisture errors must be larger in the Southern Hemisphere due to the lack of moisture information from radiosondes.

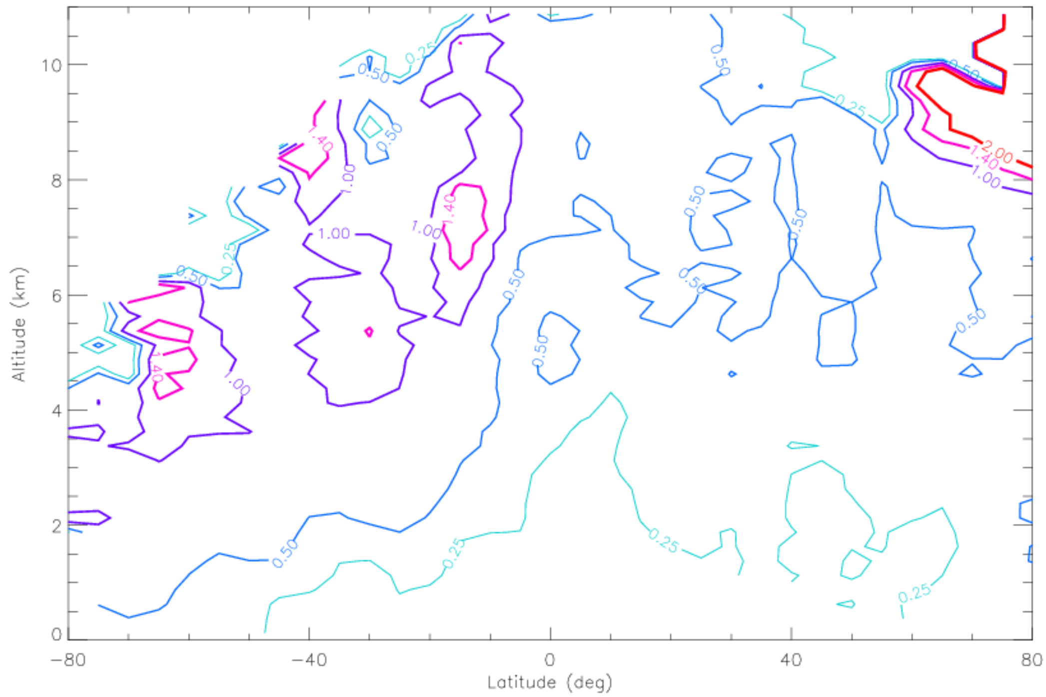

Figure 11: Estimated normalized standard deviation of the ECMWF specific humidity errors

3.6 Estimation of $\overline{q'\varepsilon'_G}$ - $\overline{q'\varepsilon'_E}$

The two variance estimates from (5a) and (5b), the variance of the specific humidity differences from (6), plus the additional constraints from the estimate of $\overline{\varepsilon_G'^2}$ and the error cross-correlation (A7) combine to provide 5 constraints. This is insufficient to uniquely define $\overline{q'\varepsilon'_G}$ and $\overline{q'\varepsilon'_E}$ independently but adequate to characterize their difference, $\overline{q'\varepsilon'_G}$ - $\overline{q'\varepsilon'_E}$ via (7b) or (7c). The resulting zonal structure of $\overline{q'\varepsilon'_G}$ - $\overline{q'\varepsilon'_E}$ and its normalized form are shown in Figures 12a and 12b.

Perhaps the most significant feature in Figure 12 is the fact that $\overline{q'\varepsilon'_G}$ - $\overline{q'\varepsilon'_E}$ is positive throughout most of the troposphere suggesting that a combination of negative $\overline{q'\varepsilon'_E}$ and positive $\overline{q'\varepsilon'_G}$ exists in general. A positive correlation implies the GPS data overestimates variations when they occur. Although it is not obvious, it is at least conceivable that occultation data could overestimate the true variations in certain situations and create some positive correlation through the data's high sensitivity to sharp vertical refractivity gradients.

A negative correlation between the true variations and the errors is expected whenever observations or analyses smooth over real variations. Figure 13 shows a schematic example of such behavior. The solid line on the right of Figure 13 shows the true specific humidity profile which includes a perturbation (shown as the dotted line to the left) relative to the mean at 4 km altitude. The dotted line on the right shows the vertically-smoothed, low resolution estimate of the truth. The solid line on the left shows the error in the smoothed profile which is the difference between the smoothed profile and the truth. The anti-correlation between the true perturbation and the error in the smoother profile is quite evident near 4 km altitude. As the example in Figure 13 shows, smoothing out the true behavior systematically produces a negative $\overline{q'\varepsilon_q'}$ term. Since TOVS provides 3 moisture radiances that span much of the troposphere whereas moisture is known to vary on much smaller vertical scales, a negative correlation between the moisture analysis errors and true variations is expected. Our results reveal indications of the anti-correlation because the GPS observations provide much higher vertical resolution than TOVS.

The smoothing in the horizontal dimension associated with the ~250 km along-track averaging interval of the occultations can also produce a negative correlation between errors and true variations. However, the horizontal resolution of the ECMWF analyses is probably not a lot better than the along-track averaging of the GPS observations and the generally positive sign of $\overline{q'\varepsilon'_G}$ - $\overline{q'\varepsilon'_E}$ suggests the vertical smoothing of the ECMWF analyses is dominating the behavior of $\overline{q'\varepsilon'_G}$ - $\overline{q'\varepsilon'_E}$. We will discuss implications of the $\overline{q'\varepsilon'_G}$ - $\overline{q'\varepsilon'_E}$ correlation behavior further in Section 5.

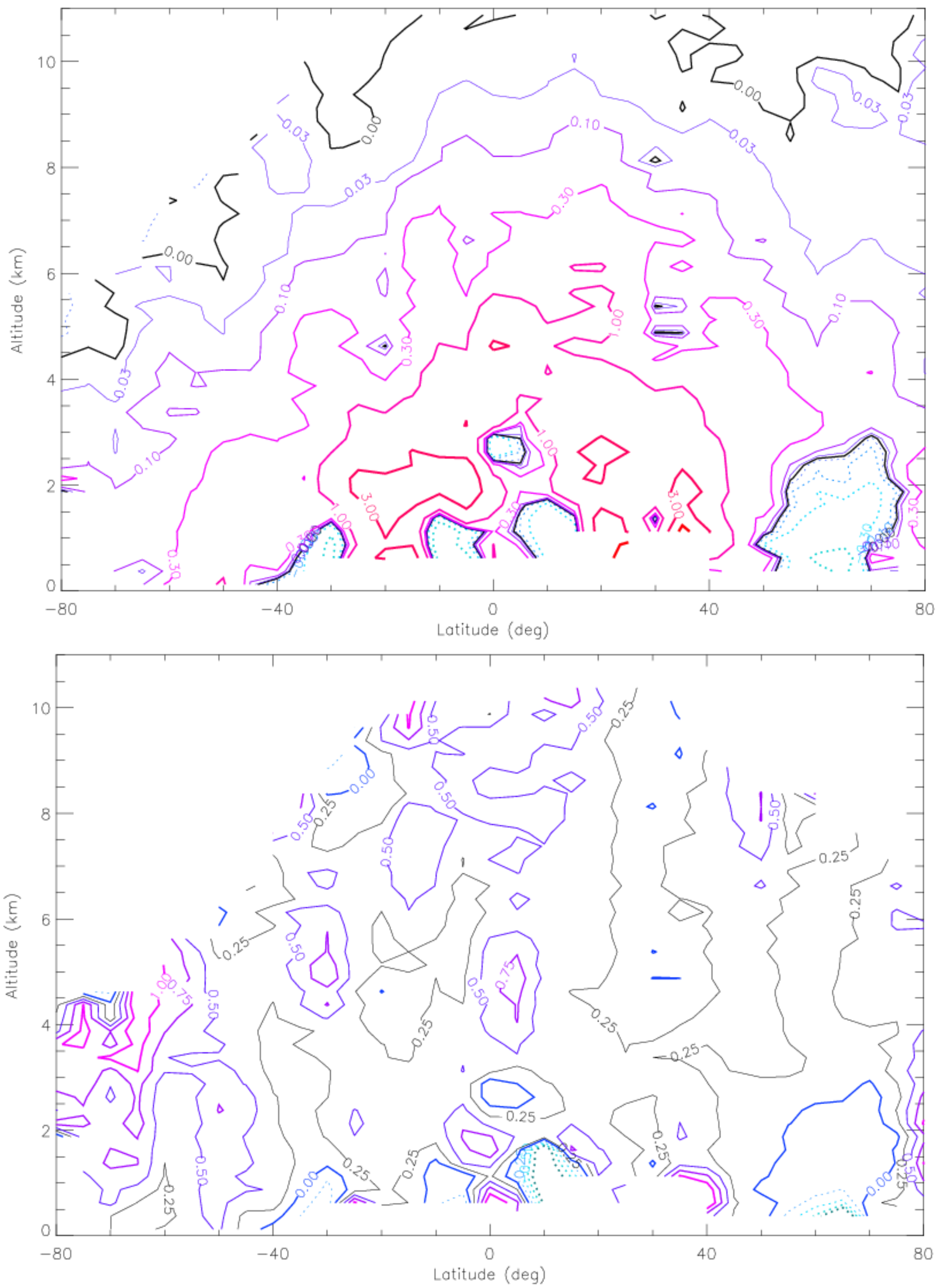

Figure 12. The difference between the correlation between the GPS moisture errors and true moisture variability and that between the ECMWF errors and the true variability. a. $\overline{q'\varepsilon'_G} - \overline{q'\varepsilon'_E}$ in $(g/kg)^2$. b. normalized by the q variance.

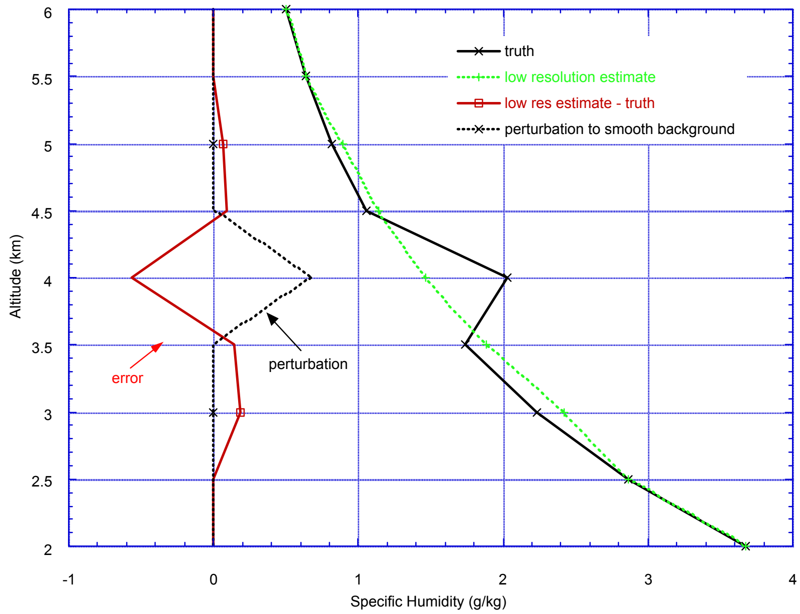

Figure 13: Schematic example of how vertical smoothing produces a negative correlation between the error and the real perturbation.

The magnitude of $\overline{q'\varepsilon'_G}$ - $\overline{q'\varepsilon'_E}$ is quite large amounting to 25 to 50% of the zonal variance of the atmospheric moisture. This suggests that the ECMWF moisture analyses are missing a large fraction of the moisture variations in the vertical dimension.

4. Improved Estimate of the True Zonal Moisture Variability, σ_q

We can now utilize the estimates of $\overline{\varepsilon'^2_G}$ and $\overline{\varepsilon'^2_E}$ and the various correlations to derive a better estimate of the true moisture variability. We write the optimal estimate of q ($\equiv q_O$) as a linear combination of q_G and q_E

$$q_O = A\, q_G + (1 - A)\, q_E \tag{13}$$

The non-mean portion of the error in (13) is $\varepsilon'_o = \varepsilon'_E + A(\varepsilon'_G - \varepsilon'_E)$ and the error variance of (13) is therefore

$$\overline{\varepsilon'^2_o} = \overline{\varepsilon'^2_E} + 2A\overline{\varepsilon'_E(\varepsilon'_G - \varepsilon'_E)} + A^2\overline{(\varepsilon'_G - \varepsilon'_E)^2} \quad = \quad \overline{\varepsilon'^2_E} + 2A\overline{\varepsilon'_E(\varepsilon'_G - \varepsilon'_E)} + A^2\sigma^2_{\Delta y} \tag{14}$$

The optimal estimate of the true variance is obtained by minimizing the magnitude of (14). Note that depending on the magnitudes and signs of the correlation terms, (14) can represent one of two situations, the first where $\overline{\varepsilon'^2_o}$ is strictly positive and the second where $\overline{\varepsilon'^2_o}$ can be positive or negative. In the first case, the solution for A that minimizes $\overline{\varepsilon'^2_o}$ is

$$A = \frac{\overline{\varepsilon'^2_E} - \overline{\varepsilon'_E\varepsilon'_G}}{\sigma^2_{\Delta q}} \tag{15}$$

In the second case there are in general two values of A that are solutions to $\overline{\varepsilon_o'^2} = 0$. The values are

$$A = \frac{\overline{\varepsilon_E'^2} - \overline{\varepsilon_E'\varepsilon_G'} \pm \sqrt{\left(\overline{\varepsilon_E'^2} - \overline{\varepsilon_E'\varepsilon_G'}\right)^2 - \sigma_{\Delta q}^2\,\overline{\varepsilon_E'^2}}}{\sigma_{\Delta q}^2} \tag{16}$$

We choose the sign in (16) based on the error variances. If $\overline{\varepsilon'^2_E} > \overline{\varepsilon'^2_G}$, the positive sign is chosen giving more weight to q_G. Otherwise, the negative sign is chosen increasing the weight of q_E.

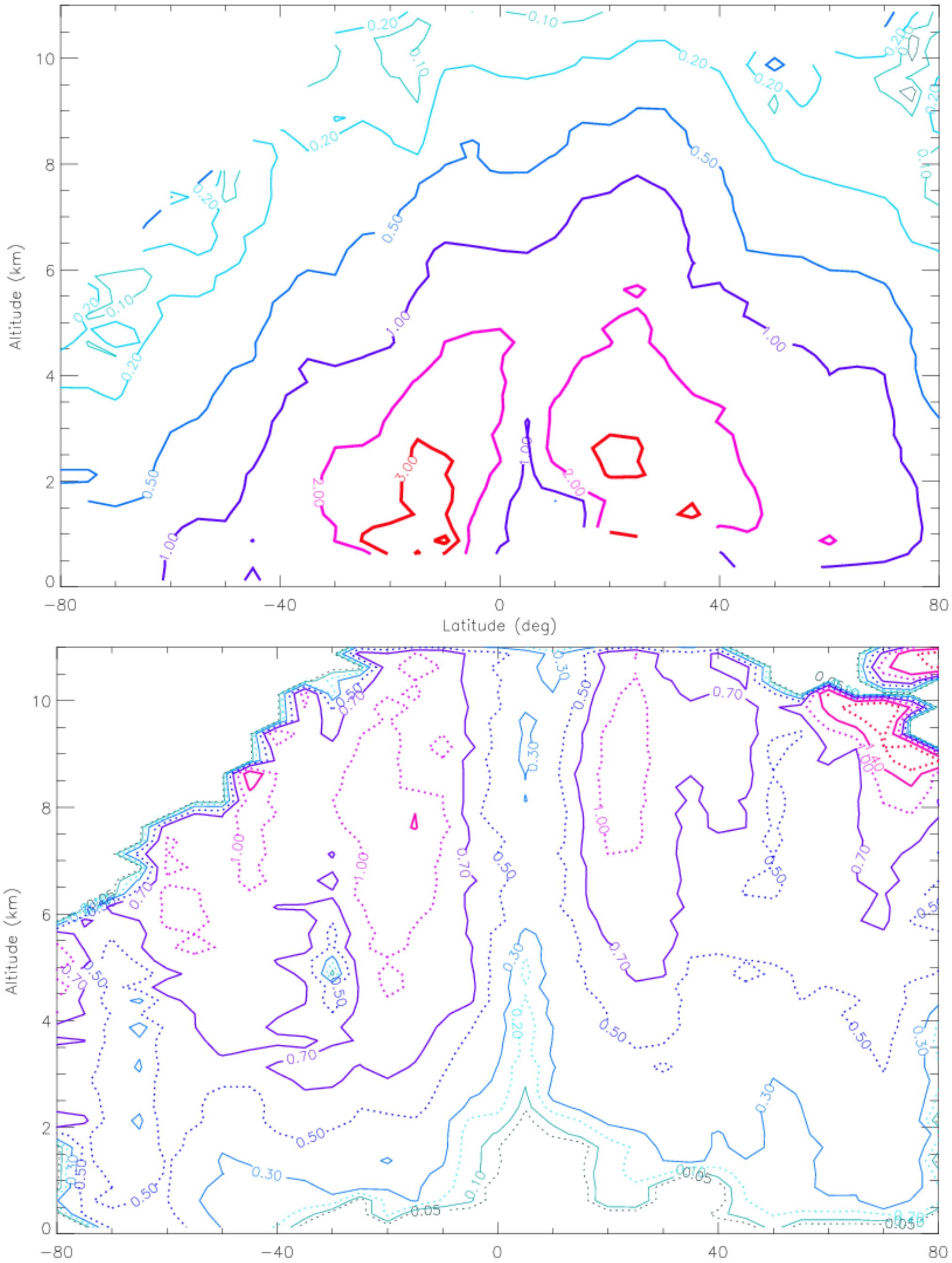

Figure 14: Optimal estimate of σ_{qo} in g/kg derived from weighted sum of GPS and ECMWF q estimates. a. σ_{qo} in g/kg. b. $\sigma_{qo}/\overline{q}$.

Figure 14a shows our best estimate of the square root of $\overline{q_o'^2} = \sigma_{qo}^2$ and Figure 14b shows σ_{qo} normalized by the zonal mean q. Figure 15 shows the zonal dependence of the weighting factor, *A,* used to derive q_o. Figure 16 shows the estimated improvement of q_o over q_E represented as the ratio of the standard deviation of the q_o error to the error in the original q_E estimate of q. The error has been reduced to less than 50% of the ECMWF analysis error over much of the troposphere. The improvement near the surface is often not quite as large because the ECMWF errors are smallest near the surface. Despite the low humidities in the wintertime Southern Hemisphere, the improvement in the Southern Hemisphere is larger than many predictions [e.g. *Healy and Eyre*, 2000] because our analysis indicates that the ECMWF moisture errors in the Southern Hemisphere are significantly larger than their Northern Hemisphere counterparts.

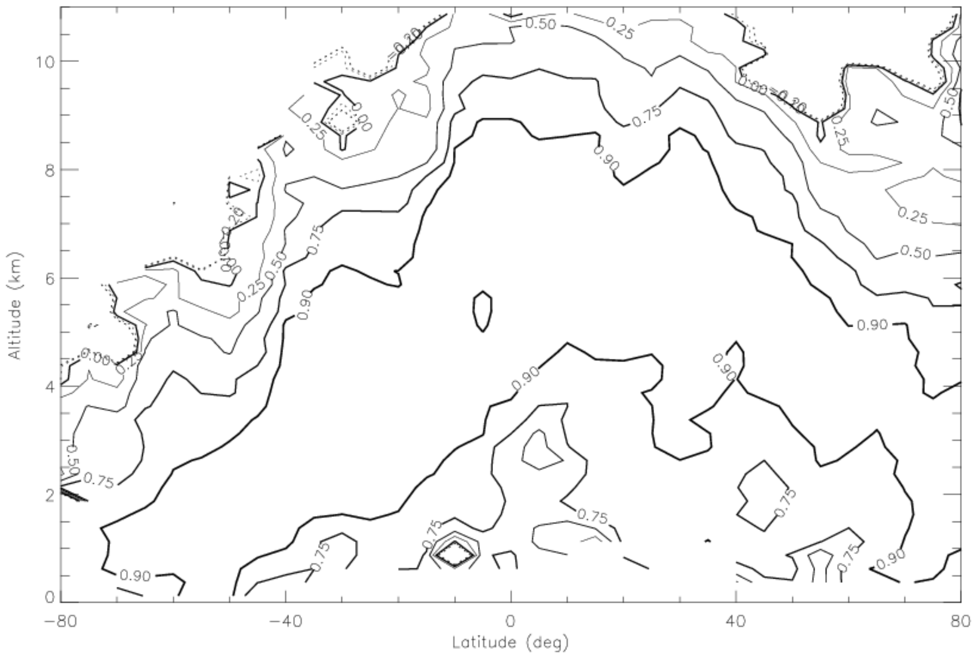

Figure 15: Weighting factor, *A*, defined in (13)-(16) and used to determine the optimal estimate of *q*.

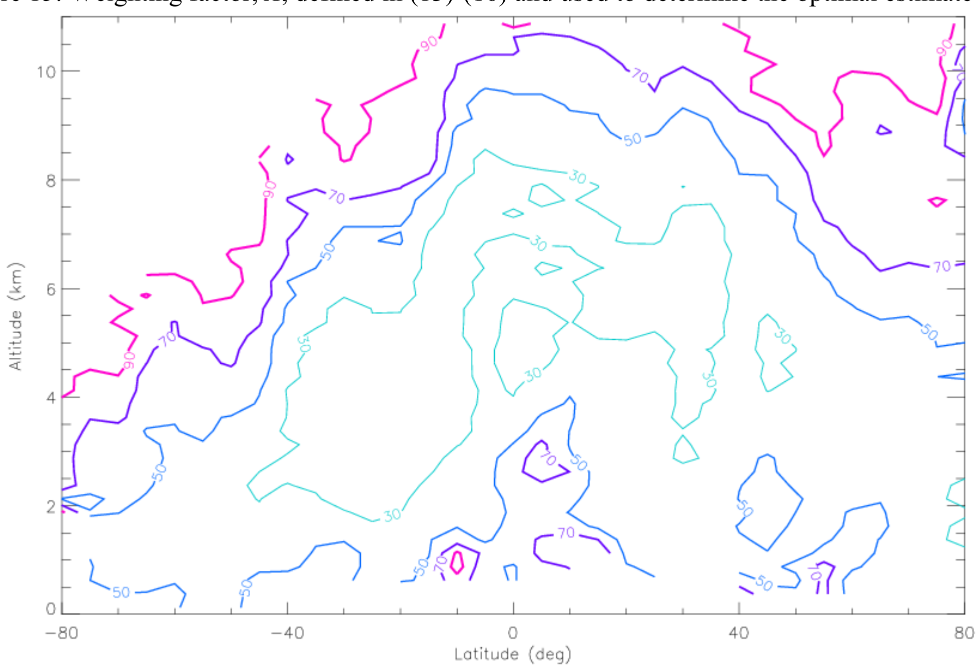

Figure 16: Ratio of standard deviation of minimum moisture error to standard deviation of ECMWF moisture error

5. Discussion of Results

We now discuss briefly the zonal variability structure armed with our improved understanding of the noise/accuracy. A full discussion of the explanation for the zonal variability requires a 3D examination of the moisture structure which is beyond the scope of the present effort.

The latitude versus height structure of the standard deviation of specific humidity variations about the zonal mean reveals a distinct pattern with a minimum centered roughly on the ITCZ near 5^{o}N and a maximum to the north and to the south peaked in the subtropics. This bi-modal meridional structure in zonal variability of q has been described by *Pexioto and Oort* [1992]. The variability seen here is somewhat larger. The ITCZ is readily apparent as a region of low zonal variability throughout the vertical range of the data, particularly in terms of the *fractional* variability (Figure 14b). At the ITCZ, the mean relative humidity plus the fractional standard deviation of the moisture variations sum to about 80%. Thus the typical conditions in the ITCZ while more moist than the regions to the north and south are not often at saturation at least at the scales resolvable by the ECMWF and GPS data. This is presumably because the convective upwellings cover a small fraction of the tropical area.

The northern and southern variability maxima correspond roughly to the subtropical zones of subsiding air. The high variability reflects longitudinal variations in the specific humidity. Both peaks in moisture variability extend upward to at least 10 km altitude. The Northern maximum peak is centered between 20^{o}N and 25^{o}N in the lower troposphere and shifts somewhat northward at higher altitudes. The northward shift and more meridionally spread maximum at higher altitudes likely reflects the influence of the Indian-Asian monsoon at higher altitudes. In the Southern Hemisphere, there is a corresponding maxima between 15^{o}S and 20^{o}S below 2.5 km altitude which shifts distinctly equator-ward to 0 to 10^{o}S at higher altitudes. The greatest variability occurs between 10^{o}S and 20^{o}S below 2.5 km altitude near the tradewind inversion in the southern descending branch of the Hadley circulation and some of the large moisture variability may be contributed by variations in the tradewind inversion height.

We note that the fractional variations are significantly smaller near the surface than in the free troposphere (Figure 14b). We also note that while the absolute variability is generally smaller in the Southern Hemisphere (Figure 14a), the fractional variability is actually larger in the Southern Hemisphere (Figure 14b). In terms of fractional variability ($\sigma_q/\overline{q}$), the Northern and Southern peaks are greater than 100% and lie between 6 and 10 km altitude. The southern fractional variability peak is distinctly southward from the absolute variability maximum associated with an interval of very dry air near 20^{o}S in the mid and upper troposphere. In regions where the standard deviation of the moisture variations divided by the zonal mean moisture is ~100% or more, the moisture distribution must be significantly skewed toward the positive end. That is the tail of the distribution must be longer on the positive side of the mean. Therefore, there must be a significant number of moisture structures whose specific humidity is more than 1σ greater than the mean.

The differences between the GPS and ECMWF variability estimates in Figure 4 deserve some attention. At low latitudes, σ_{qG} is greater than σ_{qE} (Figure 4) over much of the tropics and subtropics particularly below 4 km altitude. The variance difference is large, being 20 to more than 50% of the average of the GE and IE variance estimates. Based on the positive sign of $\overline{q'\varepsilon'}_G$ - $\overline{q'\varepsilon'}_E$ through much of this region, it also appears that there is significant negative correlation between the ECMWF errors and the true moisture variability. This suggests that σ_{qG} is greater than σ_{qIE} because substantial variations in humidity exist at vertical scales better resolved in the occultation limb-viewing geometry than in the TOVS radiances and ECMWF analyses.

In the interval between 50°N and 70°N, σ_{qE} is greater than σ_{qG} and $\overline{q'\varepsilon'_G}$ - $\overline{q'\varepsilon'_E}$ is negative. This suggests the GPS results may be smoothing our real behavior presumably in the horizontal dimension. This could indeed be the case if the ECMWF moisture information is coming primarily from radiosondes which are relatively densely spaced in this latitude band.

Over a large fraction of the winter storm region in the Southern Hemisphere, σ_{qIE} is greater than σ_{qG} with the largest discrepancy occurring near 35°S. The discrepancy suggests a combination of overestimate by the ECMWF analyses and underestimate by the occultation results. Horizontal smoothing associated with the ~250 km averaging occultation limb-viewing geometry could produce such an underestimate. However, the horizontal correlation length of moisture associated with the synoptic scale winter storm systems is generally large which occultations should generally be able to resolve. Furthermore, if horizontal smoothing were the dominant source of the variance difference, the sign of $\overline{q'\varepsilon'_G}$ - $\overline{q'\varepsilon'_E}$ would be negative and our estimate of $\overline{q'\varepsilon'_G}$ - $\overline{q'\varepsilon'_E}$ is generally positive in this region suggesting that the variability bias is due to an overestimate of variability in the analyses. This conclusion is somewhat surprising given concerns that IR observations will miss extremely moist events associated with clouds and will therefore underestimate variability. However, the actually behavior of the analyses depends on what the underlying analysis model does in the absence of observations.

6. SUMMARY AND CONCLUSIONS

We examined the zonal variability of moisture analyses over a two week period in June-July 1995 using the ECMWF humidity analyses and water vapor derived by combining GPS/MET refractivity and ECMWF temperature. This effort complemented our previous examination of zonal mean moisture [*Kursinski and Hajj,* 2001]. We found that the zonal variability of the ECMWF and GPS moisture results (defined as the standard deviation about the zonal mean) were similar with GPS observing larger variations at low latitudes and ECMWF generally seeing somewhat larger at higher latitudes. We found that large discrepancies existed between the individual profiles particularly in the Southern Hemisphere. Our effort here focused largely on untangling the error contributions to understand the cause of the large discrepancies.

We found there are significant correlations between the errors themselves and between the errors and the true moisture variability. Because we found significant correlation terms, to separate the error contributions and the true variability we had to add two extra constraints, estimate of GPS moisture accuracy and the correlation between the GPS and ECMWF moisture estimates. To estimate the GPS moisture accuracy, we estimated the standard deviation of the ECMWF temperature errors in the mid-to upper troposphere based on discrepancies between the GPS and ECMWF results. We found that the standard deviation of ECMWF temperature errors were ~1.5 K in the Northern hemisphere, ~1K at low latitudes and 1.5-2.5K over much of the Southern Hemisphere, values that are generally consistent with expectations. We then combined the temperature error estimate in combination with the approach of *Kursinski et al.* [1995] to estimate the accuracies of the moisture estimates derived from the GPS occultation data.

To estimate the correlation between the GPS and ECMWF humidity errors due to the common ECMWF temperature error, we derived an expression based upon the simplified radiative transfer equation of *Soden and Bretherton* [1996] that relates relative humidity, and brightness temperature. The magnitude of the resulting error cross-correlation explained most of the observed high altitude error cross-correlation supporting the validity of the expression.

Using the estimates of the error cross-correlation term, the GPS error and the observations themselves, we were able to estimate the error in the ECMWF humidity analyses. We found the standard deviation of ECMWF moisture errors in the Northern Hemisphere are in general agreement with the diagonal terms of error covariances used by global data assimilation systems [*e.g. Kursinski et al*., 2000] with ~25% accuracies near the surface increasing to ~50% in the mid-troposphere. However, the ECMWF moisture analysis accuracies were dramatically worse south of the equator with errors typically 2 to 3 times worse than their Northern Hemisphere counterparts.

We also discovered that significant correlations exist between the data errors and the true moisture variability. Specifically we found that $\overline{q'\varepsilon'_G} - \overline{q'\varepsilon'_E}$ was positive over most of the troposphere and its magnitude was 25 to 50% of the actual specific humidity variance over most of the troposphere. We argued that the simplest and most obvious explanation for this behavior is the ECMWF errors are anti-correlated with true variations because they are smoothing out significant vertical variations in the moisture structure. This further suggests that the reason for larger moisture variability in the GPS results at low latitudes is the ECMWF vertical smoothing is removing a substantial fraction of the true variability.

Based on our estimates of the GPS and ECMWF errors, we found that inclusion of the GPS occultation data will reduce the ECMWF moisture errors by factors of 2 to 3 over much of the lower half of the troposphere. The impact in the Southern (winter) Hemisphere was larger than anticipated because of the substantially lower ECMWF accuracies we found there.

The latitude versus height structure of the specific humidity variations is generally similar to that described by Peixioto and Oort [1992] with a distinct minimum at the ITCZ and relative maximum variability to the north and south centered approximately in the subtropics. Fractional variability is substantially larger 6 to 10 km above the surface in the free troposphere.

At low latitudes, the occultation data revealed moisture variances 20 to 50% higher than the ECMWF analyses. In contrast, in the Southern Hemisphere, the ECMWF humidity analyses exhibit more variability than the GPS results. The cause for the discrepancy could be an overestimate in the analyses or an underestimate in the GE results due to horizontal smoothing. Since the sign of $\overline{q'\varepsilon'_G} - \overline{q'\varepsilon'_E}$ is positive, the variability difference may be due to an overestimate of variability in the ECMWF analyses. There is also an interval in the Northern hemisphere in which the ECMWF variability is larger than the GPS estimates and $\overline{q'\varepsilon'_G} - \overline{q'\varepsilon'_E}$ is negative. It may be that the assimilation of radiosonde data by the ECMWF analyses explains the results in this region. As a result, the ECMWF analyses may contain more variability at smaller horizontal scales than the GPS observations which would explain both σ_E being greater than σ_G and $\overline{q'\varepsilon'_G} - \overline{q'\varepsilon'_E}$ being negative.

These results are for the 1995 version of the ECMWF analyses. We have begun extending this analysis of global moisture variability to utilize the much larger data sets being generated by the GPS occultation receivers on the CHAMP and SAC-C spacecraft [*Hajj et al*., 2002]. The larger and improved data sets should allow a full 3D examination by season together with still higher GPS vertical resolution through the application of backpropagation and canonical transform concepts [e.g. *Gorbunov*, 2002] which improve the vertical resolution of the GPS results to ~200 m.

APPENDIX: CORRELATION BETWEEN SPECIFIC HUMIDITY ESTIMATES FROM GPS AND ECMWF ANALYSES.

We are interested in estimating the accuracy of the ECMWF humidity fields given the ECMWF and GPS results and estimated GPS accuracy. The mean square of the difference between the GE and IE specific humidity (q) results is

$$\overline{(q_G - q_E)^2} = \overline{\left([q + \varepsilon_G] - [q + \varepsilon_E]\right)^2} = \overline{(\varepsilon_G - \varepsilon_E)^2}$$

$$= \overline{\varepsilon_G{}^2} - 2\,\overline{\varepsilon_G \varepsilon_E} + \overline{\varepsilon_E{}^2}$$

The mean square error of the ECMWF humidities is

$$\overline{\varepsilon_E{}^2} = \overline{(q_G - q_E)^2} - \overline{\varepsilon_G{}^2} + 2\,\overline{\varepsilon_G \varepsilon_E} \tag{A1}$$

Were the GPS and ECMWF moisture data sets independent, the correlation term would be zero and could be ignored. Humidity derived from refractivity uses temperature from weather analyses such as the ECMWF global 6 hour analyses and the accuracy of the water vapor results depends on the accuracy of the ECMWF temperature. The global humidity field in the ECMWF analyses is derived largely from TOVS radiances which requires knowledge of temperature as well. Therefore errors in the two humidity estimates are correlated and $\overline{\varepsilon_G^{'} \varepsilon_E^{'}} \neq 0$.

Following the approach of *Kursinski et al.*, [1995] and *Kursinski and Hajj* [2001], the dependence of specific humidity derived from GPS observations on refractivity, temperature and pressure is

$$\frac{dq}{q} = (B+1)\frac{dN}{N} + (B+2)\frac{dT}{T} - (B+1)\frac{dP}{P}$$

where $B = b_1\, T\, m_w / b_2\, q\, m$ and $b_1 = 77.6$ K/mbar and $b_2 = 3.73 \times 10^5$ K^2/mbar. Refractivity does not depend on the analysis temperature. Pressure does. However, near the 230 K isotherm, pressure is derived primarily from the occultation refractivity data. At lower altitudes it will turn out that the contribution of the correlation term is insignificant and the pressure contribution can therefore be ignored. Further, near the 230 K isotherm, $B \gg 1$ so that

$$\frac{\partial q}{q\,\partial T} \cong \frac{(B+2)}{T} \cong \frac{b_1 m_w}{b_2 m q} \tag{A2}$$

Therefore the absolute (versus fractional) error in q due to temperature error is linearly proportional to the error in T with a scale factor of ~0.13 g kg^{-1}K^{-1}.

To avoid the complexity of the radiative transfer coupling between humidity and temperature in the analyses, we will utilize the framework developed by *Soden and Bretherton* [1996], for interpreting GOES and TOVS radiances in terms of humidity. Conceptually, brightness temperature represents a layer average relative humidity that can be represented as

$$a + b\,T_b = \log_e\left(\frac{r\ p_o}{\beta\ \cos\theta}\right)$$

where the variables are brightness temperature T_b, relative humidity r, normalized lapse rate β, reference pressure p_o which is equal to the pressure at the 240 K isotherm divided by 300 mbar ($p_o = P[T{=}240$ K$]/300$ mbar). The constants, a and b, depend on the TOVS channel being used. We are interested in how derived humidity depends on temperature. Since T_b is observed, β is roughly constant and θ is determined by observational geometry, only r and p_o can vary with temperature, T. Therefore as T is varied, the product, $r\,p_o$, must remain constant.

$$\frac{dr}{r\,dT} = -\frac{d\,p_o}{p_o\,dT}$$

r can be written in terms of q as

$$r = \frac{e}{e^*} = \frac{q\,P\,m}{e^*\,m_w}$$

where e is vapor pressure, e^* is saturation vapor pressure, P is the air pressure, m is mean molecular mass of the air and m_w is the mean molecular mass of water vapor. Therefore the variation of r with T is

$$\frac{dr}{r\,dT} = \frac{dq}{q\,dT} - \frac{de^*}{e^*\,dT}$$

The variation of q with T is

$$\frac{dq}{q\,dT} = \frac{dr}{r\,dT} + \frac{de^*}{e^*\,dT} = -\frac{d\,p_o}{p_o\,dT} + \frac{de^*}{e^*\,dT} \tag{A3}$$

$p_o = P(T)/300$ mbar. To estimate the change in p_o due to a temperature error we note that *Soden and Bretherton* argue that the normalized lapse rate $\beta = P/T\ \mathrm{d}T/\mathrm{d}P = \mathrm{dln}T/\mathrm{dln}P$ can be taken as constant such that T and P are related approximately as

$$\frac{T}{T_{ref}} = c\left(\frac{P}{P_{ref}}\right)^{\beta}$$

The case we are interested in is the change in $P(T)$ when P_{ref} and T are held constant and $T_{ref} = T(P_{ref})$ is changed. The resulting change in $P(T)$ is

$$\frac{dP}{P} = -\frac{1}{\beta}\frac{dT_{ref}}{T_{ref}}$$

so that

$$\frac{d\,p_o}{p_o\,dT_{ref}} = \frac{dP}{P\,dT_{ref}} = -\frac{1}{\beta\,T_{ref}} \tag{A4}$$

Concerning the second term on the RHS of (A3), from the Clausius-Clapeyron relation

$$\frac{de^*}{e^*\,dT} = \frac{0.622\,L}{R\,T^2} \tag{A5}$$

where R is the dry gas constant (= 287 J kg^{-1} K^{-1}) and L is the latent heat of sublimation or evaporation. Using (A4) and (A5), (A3) becomes

$$\frac{dq}{q\,dT} = \frac{1}{\beta\,T} + \frac{0.622\,L}{R\,T^2} \tag{A6}$$

Note that the second term is roughly 5 times greater than the first term. Note also that the variation in the fractional change across the troposphere in q due to an error in T is small in comparison to the variation in the GPS estimate.

Combining (A2) and (A6), the correlation term in (A1) can be written as

$$\frac{\overline{\varepsilon_G\,\varepsilon_E}}{q^2} = \frac{b_1\,m_w}{b_2\,m\,q}\left(\frac{1}{\beta\,T} + \frac{0.622\,L}{R\,T^2}\right)\overline{\varepsilon_T^2} \tag{A7}$$

Note that all terms are positive so the correlation is positive. With the exception of q, the variables on the RHS of (A7) vary little with height, and the fractional correlation term error will grow exponentially with height with the scale height of water vapor. Inserting (A7) into (A1) yields

$$\overline{\varepsilon_E^{\,2}} = \overline{(q_G - q_E)^2} - \overline{\varepsilon_G^{\,2}} + 2\,\frac{b_1\, m_w\, q}{b_2\, m}\left(\frac{1}{\beta\, T} + \frac{0.622\, L}{R\, T^2}\right)\overline{\varepsilon_T^2} \tag{A8}$$

To estimate $\overline{\varepsilon_E^{\,2}}$, we use the data to calculate the first term on the RHS of (A8) and estimate the second and third terms based on *apriori* information as well as the comparison of the two data sets.

Acknowledgement: This work was supported in part by the NASA Cal-Val program and the National Polar Orbiting Environmental Satellite System (NPOESS).

REFERENCES

Gorbunov, M. E., 2001, Radioholographic methods for processing radio occultations data in multipath regions, Scientific Report 01-01, Danish Meteorological Institute, Copenhagen.

Hajj, G.A., M. de la Torre Juarez, B. Iijima, E. R. Kursinski, A. Mannucci, T. P. Yunck, GPS Radio Occultations Coming of Age, *EOS*, **83**, No. 4, p. 37, Jan. 22, 2002.

Healy, S. B., 2001, Radio occultation bending angle and impact parameter errors caused by horizontal refractive gradients in the troposphere: a simulation study, *J. Geophys. Res*., **106**, 11875-11889.

Healy S. B., and J. R. Eyre, 2000, Retrieving temperature, water vapour and surface pressure information from refractive-index profiles derived by radio occultation: A simulation study, *Q. J. R. Met. Soc*., **126**, 1661-1683.

Kursinski, E.R., G.A. Hajj, K.R. Hardy, L.J. Romans and J.T. Schofield, Observing tropospheric water vapor by radio occultation using the Global Positioning System, *Geophys. Res. Lett.*, **22**, 2365-2368, 1995.

Kursinski, E. R., G. A. Hajj, J. T. Schofield, R. P. Linfield and K. R. Hardy, Observing Earth's atmosphere with radio occultation measurements using the Global Positioning System, *J. Geophys. Res.,* **102**, 23429-23465, 1997.

Kursinski, E. R., S. B. Healy and L. J. Romans, Initial Results of Combining GPS Occultations with ECMWF Global Analyses within a 1Dvar Framework, *Earth, Planets and Space*, **52**, 885-892, 2000.

Kursinski, E. R. and G. A. Hajj, A comparison of water vapor derived from GPS occultations and global weather analyses, *J. Geophys. Res.,* **106**, 1113-1138, 2001.

Peixoto, J. P., and A. H. Oort, *Physics of Climate*, 520 pp., Am. Inst. Phys, New York, 1992.

Poli, P., J. Joiner, and E. R. Kursinski, 1Dvar analysis of temperature and humidity using GPS radio occultation data, *in press J. Geophys. Res.,* 2002.

Smith, E. K., and S. Weintraub, The constants in the equation for atmospheric refractive index at radio frequencies, *Proc. IRE, 41*, 1035-1037, 1953.

Soden, B. J., and F. P. Bretherton, Interpretation of TOVS water vapor radiances in terms of layer-average relative humidities: Method and climatology for the upper, middle and lower troposphere, *J. Geophys. Res*., **101**, 9333-9343, 1996.

Ware, R., et al., GPS sounding of the atmosphere from low Earth orbit - preliminary results, *Bull. Am. Meteorol. Soc., 77*, 19-40, 1996.